

Jet spectra in FRI radio galaxies: implications for particle acceleration

R.A. Laing

*ESO, Karl-Schwarzschild-Straße 2, 85748 Garching-bei-München,
Germany*

A.H. Bridle, W.D. Cotton

NRAO, 520 Edgemont Road, Charlottesville, VA 22903-2475, U.S.A.

D.M. Worrall, M. Birkinshaw

*Department of Physics, University of Bristol, Tyndall Avenue, Bristol
BS8 1TL, U.K.*

Abstract. We describe very accurate imaging of radio spectral index for the inner jets in three FRI radio galaxies. Where the jets first brighten, there is a remarkably small dispersion around a spectral index of 0.62. This is also the region where bright X-ray emission is detected. Further from the nucleus, the spectral index flattens slightly to 0.50 - 0.55 and X-ray emission, although still detectable, is fainter relative to the radio. The brightest X-ray emission from the jets is therefore not associated with the flattest radio spectra, but rather with some particle-acceleration process whose characteristic energy index is 2.24. The change in spectral index occurs roughly where our relativistic jet models require rapid deceleration. Flatter-spectrum edges can be seen where the jets are isolated from significant surrounding diffuse emission and we suggest that these are associated with shear.

1. Radio spectra: 3C 31

The detection of X-ray synchrotron emission on kiloparsec scales in the bases of low-luminosity (FRI) radio jets (e.g. Hardcastle et al. 2002, 2005; Worrall et al. 2007) requires distributed particle acceleration, consistent with the failure of adiabatic models to reproduce the observed brightness profiles at radio wavelengths (Laing & Bridle 2004). The acceleration mechanism is not understood. Here, we summarize the results of recent work on this problem, using accurate radio spectral mapping (this section) and detailed radio – X-ray comparisons (Section 2.).

In the course of our jet-modelling programme (Laing & Bridle 2007, and references therein), we have accumulated high-resolution, multi-frequency radio images of the bases of FRI jets and have used these to derive accurate spectral-index distributions. We have studied NGC 315 (Laing et al. 2006a) and 3C 296 (Laing et al. 2006b); a third example, the nearby radio galaxy 3C 31 ($z = 0.0169$; Laing et al., in preparation), is shown in Fig. 1. There is no evidence for any significant deviation from power-law spectra in 3C 31 within 70 arcsec of the nu-

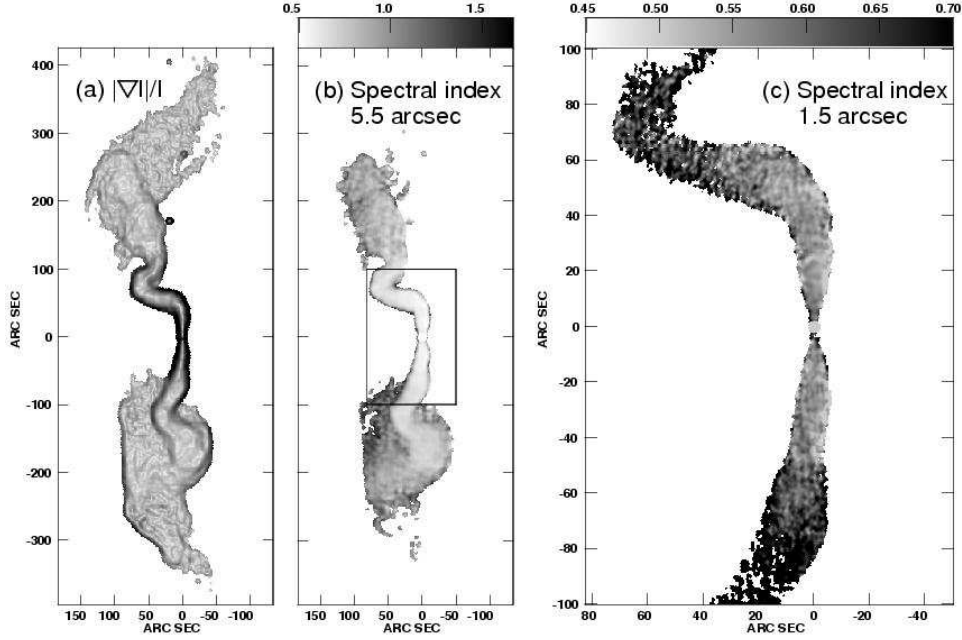


Figure 1. Radio images of 3C 31. (a) Sobel-filtered, mean L-band image (normalized by total intensity) at a resolution of 5.5 arcsec. (b) and (c) Spectral index, α from weighted least-squares, power-law fits to the total intensity. (b) 5-frequency fit between 1365 and 4985 MHz at a resolution of 5.5 arcsec FWHM. (c) 6-frequency fit between 1365 and 8440 MHz at a resolution of 1.5 arcsec FWHM for the inset area in panel (b).

clous. Out to ≈ 7 arcsec in both jets, the spectral index at 1.5-arcsec resolution is slightly steeper ($\langle \alpha \rangle = 0.62$)¹ than the average for the inner jets. From 7 – 50 arcsec in both jets, the mean spectral index is in the range 0.55 – 0.57. Further from the nucleus, there is a gradual spectral steepening. There are also slight, but significant variations in spectral index across both jets within ≈ 30 arcsec of the nucleus in the sense that their West edges tend to have flatter spectra ($\langle \alpha \rangle = 0.52 - 0.54$; Fig. 1c). There is a clear spectral separation between the South jet and the surrounding emission, matching the separation of these regions defined by the sharpest brightness gradients (Figs 1a and b). This is particularly clear where the jet first enters the diffuse emission. The spectral identity of the jet is evidently maintained even after it bends abruptly about 2 arcmin South of the nucleus and remains until it terminates in a region of high brightness gradient. The outer South jet in 3C 31 is therefore a clear example of the type of spectral structure noted in other FRI sources (Katz-Stone & Rudnick 1997; Laing et al. 2006b) wherein a flatter-spectrum ‘jet’ with a distinct spectral identity is superposed on a ‘sheath’ of steeper-spectrum emission.

¹ $S(\nu) \propto \nu^{-\alpha}$

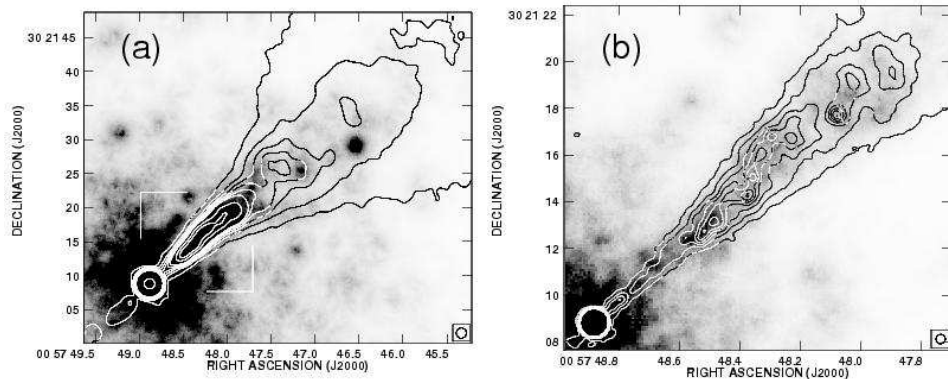


Figure 2. Overlays of VLA 5 GHz images (contours) on adaptively smoothed *Chandra* 0.8 – 5 keV data (grey-scale) for NGC 315 (Worrall et al. 2007). (a) Radio resolution 1.5 arcsec. The area covered by panel (b) is shown by the white box. (b) radio resolution 0.4 arcsec.

2. Radio – X-ray comparison: NGC 315

Comparison of deep, high-resolution radio and X-ray images also provides clues to particle-acceleration processes. Fig. 2 shows overlays of 5-GHz radio emission at resolutions of 1.5 and 0.4 arcsec FWHM on deep *Chandra* X-ray images for the main jet in NGC 315 ($z = 0.01648$; Worrall et al. 2007). The radio and X-ray spectral indices integrated over the inner jet are 0.61 and 1.2, respectively, consistent with synchrotron emission from a single population of relativistic electrons in both wavebands. The radio jet is relatively faint and unresolved in width out to about 4 arcsec from the core, after which it brightens abruptly. The most prominent feature of the radio brightness distribution between 4 and 12 arcsec (Fig. 2b) is an oscillatory filament, whose nature is discussed in detail by Worrall et al. (2007). The first X-ray enhancement which can unambiguously associated with the jet is 3.6 arcsec from the nucleus, where the radio emission is still faint. From 5 – 7.5 arcsec, there is particularly good morphological correspondence between radio and X-ray images, with diffuse emission over the full width of the jet as well as localized X-ray peaks following the radio ridge-line. At larger distances, the general correspondence is still reasonable, but there are differences of detail. The X-ray emission can be traced out to ≈ 30 arcsec (Fig. 2a), but becomes weaker with respect to the radio at ≈ 20 arcsec. This is most clearly illustrated by the profiles of X-ray and radio emission along the jet at matched resolutions in in Fig. 3; an equivalent plot for 3C 31 (Laing & Bridle 2004) is shown for comparison.

3. Discussion

These observations contribute to the developing picture of spectral variations in FRI sources. Bright X-ray emission is detected close to the nucleus, in the faint, well-collimated jet bases that precede the sudden radio brightening (e.g. Fig. 3). There is approximate morphological correspondence between features in

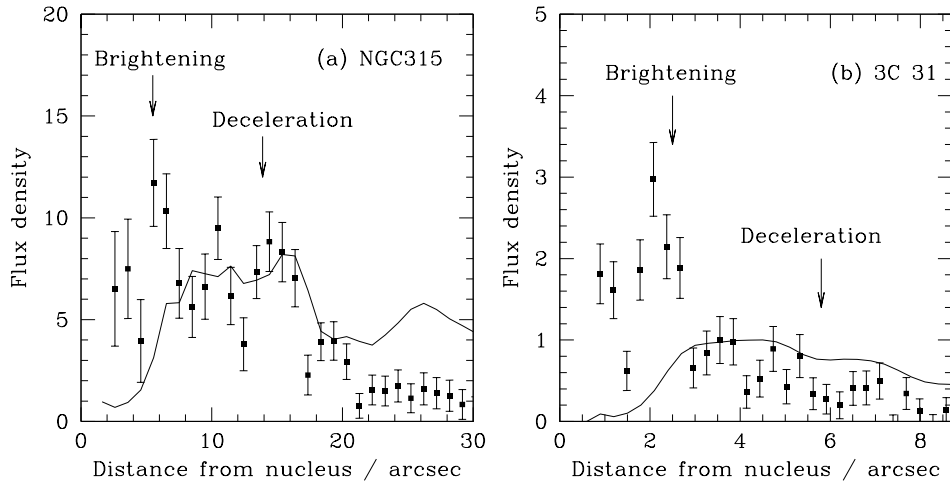


Figure 3. Profiles of radio (curve) and X-ray (points) flux density along the brighter jets of NGC 315 (Worrall et al. 2007) and 3C 31 (Laing & Bridle 2004). The locations of the brightening points (where the rest-frame radio emission increases rapidly) and the start of rapid deceleration, as modelled by Canvin et al. (2005) and Laing & Bridle (2002) are also indicated.

the radio and X-ray brightness distributions after the former brightens, although there are differences on small scales (e.g. Fig. 2b). In contrast, there are no systematic transverse variations in the X-ray/radio ratio within ≈ 30 arcsec of the nucleus in NGC 315 (the best resolved case; Worrall et al. 2007). Particle acceleration appears to be distributed throughout the jet volume, rather than being exclusively associated with discrete knots or with the boundary. The ratio of X-ray to radio emission decreases where our kinematic models show that the jets start to decelerate from speeds of $0.8 - 0.9c$ (Fig. 3; Laing & Bridle 2002; Hardcastle et al. 2002; Canvin et al. 2005; Worrall et al. 2007).

Where the jets first brighten and before they decelerate, there is a remarkably small dispersion around a radio spectral index of $\alpha = 0.62$ in the three sources we have studied in detail, as well as 3C 66B (Fig. 1; Hardcastle et al. 2001; Laing et al. 2006a,b). The average is dominated by emission immediately after the point at which the jets first brighten. This is also the region from which X-ray emission is detected from the main jets in all four sources (Fig. 3; Hardcastle et al. 2001, 2005). The spectral index of the fainter emission close to the nucleus in 3C 449 (Katz-Stone & Rudnick 1997), PKS1333–33 (Killeen, Bicknell & Ekers 1986) and 3C 66B (Hardcastle et al. 2001) appears to be slightly steeper than $\alpha = 0.62$ although the uncertainties are larger. Further from the nucleus, the spectra flatten slightly to $\alpha = 0.50 - 0.55$, contrary to any naive expectation from models in which electrons are accelerated at the brightening point and suffer synchrotron losses as they propagate. X-ray emission is still detected from these regions, but at a lower level relative to the radio (Fig. 3). The brightest X-ray emission from the jets is therefore not associated with the flattest radio spectra, but rather with some particle acceleration process whose characteristic energy index is $2\alpha + 1 = 2.24$. A related result is that an asymptotic low-frequency spectral index of 0.55 is common in FRI jets

over larger areas than we consider here (Young et al. 2005). Flatter-spectrum edges can be seen where the jets are isolated from significant surrounding diffuse emission, most clearly in NGC 315 (Laing et al. 2006a). Our kinematic models (Laing & Bridle 2002; Canvin et al. 2005; Laing et al. 2006b) show that all of the jets have substantial transverse velocity gradients and it is plausible that the process that produces the flatter spectrum is associated with high shear (Stawarz & Ostrowski 2002). In 3C 31, the flatter-spectrum regions (Fig. 1c) occur predominantly on the outer edges of bends, perhaps consistent with this idea.

As well as a smooth steepening of the jet spectrum at larger distances from the nucleus, as would be expected from synchrotron and adiabatic losses affecting a homogeneous electron population, multiple spectral components are observed (Fig. 1b). Jets appear to retain their identities even after entering regions of diffuse emission and are clearly identifiable by their flatter spectra. They are usually also separated from the surrounding emission by sharp brightness gradients (Fig. 1a). This spine/sheath separation is observed in FRI sources with bridges of emission extending back towards the nucleus (e.g. 3C 296; Laing et al. 2006b) as well as tailed sources like 3C 31 (Fig. 1). Although there is an overall trend for the spectrum of the diffuse emission to steepen towards the nucleus in bridges and away from it in tails (Parma et al. 1999), the variations in individual objects are complex. The termination regions of jets in tailed FRI sources are perhaps best regarded as bubbles which are continually fed with fresh relativistic plasma by the jets and which in turn leak material into the tails. Their spectral steepening would then be governed by a combination of continuous injection, adiabatic, synchrotron and inverse Compton energy losses and escape.

Acknowledgments. The National Radio Astronomy Observatory is a facility of the National Science Foundation operated under cooperative agreement by Associated Universities, Inc.

References

- Canvin, J.R., Laing, R.A., Bridle, A.H., Cotton, W.D., 2005, MNRAS, 363, 1223
 Hardcastle, M.J., Birkinshaw, M., Worrall, D.M., 2001, MNRAS, 326, 1499
 Hardcastle, M.J., Worrall, D.M., Birkinshaw, M., Laing, R.A., Bridle, A.H., 2002, MNRAS, 334, 182
 Hardcastle M.J., Worrall D.M., Birkinshaw M., Laing R.A., Bridle A.H., 2005, MNRAS, 358, 843
 Katz-Stone, D.M., Rudnick, L., 1997, ApJ, 488, 146
 Killeen N.E.B., Bicknell G.V., Ekers R.D., 1986, ApJ, 302, 306
 Laing, R.A., Bridle, A.H., 2007, these proceedings
 Laing, R.A., Bridle, A.H., 2002, MNRAS, 336, 328
 Laing, R.A., Bridle, A.H., 2004, MNRAS, 348, 1459
 Laing, R.A., Canvin, J.R., Cotton, W.D., Bridle, A.H., 2006a, MNRAS, 368, 48
 Laing, R.A., Canvin, J.R., Bridle, A.H., Hardcastle, M.J., 2006b, MNRAS, 372, 510
 Parma, P., Murgia, M., Morganti, R., Capetti, A., de Ruiter, H.R., Fanti, R., 1999, A&A, 344, 7
 Stawarz, L., Ostrowski, M., 2002, ApJ, 578, 763
 Worrall, D. M., Birkinshaw, M., Laing, R. A., Cotton, W. D., Bridle, A. H., 2007, MNRAS, 380, 2
 Young A., Rudnick L., Katz D., Delaney T., Kassim N.E., Makishima K., 2005, ApJ, 626, 748